TGF-β signaling in insects regulates metamorphosis via juvenile hormone biosynthesis

Yoshiyasu Ishimaru[a], Sayuri Tomonari[b], Yuji Matsuoka[a], Takahito Watanabe[c], Katsuyuki Miyawaki[c], Tetsuya Bando[d], Kenji Tomioka[e], Hideyo Ohuchi[d], Sumihare Noji[c,1], and Taro Mito[a,1]

[a]Department of Life Systems, Institute of Technology and Science, Tokushima University Graduate School, Tokushima City, Tokushima, 770-8506, Japan; [b]Division of Chemical and Physical Analyses, Center for Technical Support, Institute of Technology and Science, Tokushima University, Tokushima City, Tokushima, 770-8506, Japan; [c]Center for Collaboration Among Agriculture, Industry and Commerce, Tokushima University, Tokushima City, Tokushima, 770-8506, Japan; [d]Department of Cytology and Histology, Graduate School of Medicine, Dentistry and Pharmaceutical Sciences, Okayama University, Okayama City, Okayama, 700-8558, Japan; and [e]Department of Integrative Biology, Graduate School of Natural Science and Technology, Okayama University, Okayama City, Okayama, 700-8530, Japan

Edited by Lynn M. Riddiford, Howard Hughes Medical Institute Janelia Farm Research Campus, Ashburn, VA, and approved April 7, 2016 (received for review January 27, 2016)

Although butterflies undergo a dramatic morphological transformation from larva to adult via a pupal stage (holometamorphosis), crickets undergo a metamorphosis from nymph to adult without formation of a pupa (hemimetamorphosis). Despite these differences, both processes are regulated by common mechanisms that involve 20-hydroxyecdysone (20E) and juvenile hormone (JH). JH regulates many aspects of insect physiology, such as development, reproduction, diapause, and metamorphosis. Consequently, strict regulation of JH levels is crucial throughout an insect's life cycle. However, it remains unclear how JH synthesis is regulated. Here, we report that in the corpora allata of the cricket, *Gryllus bimaculatus*, Myoglianin (*Gb'*Myo), a homolog of *Drosophila* Myoglianin/vertebrate GDF8/11, is involved in the down-regulation of JH production by suppressing the expression of a gene encoding JH acid *O*-methyltransferase, *Gb'jhamt*. In contrast, JH production is up-regulated by Decapentaplegic (*Gb'*Dpp) and Glass-bottom boat/60A (*Gb'*Gbb) signaling that occurs as part of the transcriptional activation of *Gb'jhamt*. *Gb'*Myo defines the nature of each developmental transition by regulating JH titer and the interactions between JH and 20E. When *Gb'myo* expression is suppressed, the activation of *Gb'jhamt* expression and secretion of 20E induce molting, thereby leading to the next instar before the last nymphal instar. Conversely, high *Gb'myo* expression induces metamorphosis during the last nymphal instar through the cessation of JH synthesis. *Gb'myo* also regulates final insect size. Because Myo/GDF8/11 and Dpp/bone morphogenetic protein (BMP)2/4-Gbb/BMP5–8 are conserved in both invertebrates and vertebrates, the present findings provide common regulatory mechanisms for endocrine control of animal development.

Gryllus bimaculatus | juvenile hormone | metamorphosis | GDF8/11 | RNA interference

Holometabolous insects, such as butterflies, beetles, and flies, undergo a dramatic morphological transformation from larva to pupa to adult, a process referred to as "holometamorphosis." Hemimetabolous insects, such as locusts, cockroaches, and crickets, also undergo morphogenesis, similar to that observed in the larva-to-pupa and pupa-to-adult transitions of holometabolous insects, to form mature wings and external genitalia. However, the change of form is not drastic, because nymphs are similar to their adult form. Despite these differences in metamorphic type, both hemimetabolous and holometabolous processes are regulated by common mechanisms involving the molting steroid 20-hydroxyecdysone (20E) and the sesquiterpenoid, juvenile hormone (JH) (1–3). The latter regulates many aspects of insect physiology, such as development, reproduction, diapause, and metamorphosis (4, 5). Consequently, strict regulation of JH levels is crucial throughout an insect's life cycle. JH is synthesized in and released from the corpora allata (CA), a pair of epithelial endocrine glands in the head (6–8). It has been hypothesized that JH biosynthesis is regulated by both stimulatory (allatotropic) and inhibitory (allatostatic) neuropeptides, and JH is able to reach the glands via the hemolymph and/or nervous connections (9). However, the mechanisms regulating JH synthesis remain unclear.

Temporal transcriptional control of *jhamt*, a gene that encodes a JH acid *O*-methyltransferase that converts inactive JH precursors into active JH, is thought to be critical for regulating JH synthesis (3, 10). Furthermore, the protein JHAMT has been found to catalyze the final step of the JH biosynthesis pathway in the CA of various insects, including *Drosophila melanogaster*, *Tribolium castaneum*, *Apis mellifera*, and *Bombyx mori* (11–14). It also has been demonstrated that *jhamt* is expressed predominantly in the CA, and its developmental expression profile correlates highly with changes in JH titer. However, the molecular mechanisms underlying regulation of the temporal expression profile of *jhamt*, a long-standing area of research in entomology (10), remain unknown. To elucidate the mechanisms underlying the regulation of JH titer, the cricket *Gryllus bimaculatus* (15, 16) was used as a model system of hemimetabolous ancestors that evolved into holometabolous insects (2, 17). In the present study,

Significance

Insects undergo a morphological transformation from nymph/larva to adult with or without pupal formation, processes referred to as "hemimetamorphosis" and "holometamorphosis," respectively. Both processes are regulated by common mechanisms involving the hormones 20-hydroxyecdysone and juvenile hormone (JH). However, it remains unclear how synthesis of JH is regulated in the corpora allata (CA). Here, we report that in *Gryllus bimaculatus* the TGF-β ligands Myoglianin (*Gb'*Myo) (GDF8/11 homolog) and Decapentaplegic/Glass-bottom boat/60A (*Gb'*Dpp/Gbb) regulate JH synthesis via expression of the JH acid *O*-methyltransferase in the CA. Furthermore, loss of *Gb'*Myo function preserves the status quo action of JH and prevents metamorphosis. These findings elucidate regulatory mechanisms that provide endocrine control of insect life cycles and provide a model of GDF8/11 function.

Author contributions: Y.I. designed research; Y.I., S.T., Y.M., T.W., K.M., and T.B. performed research; Y.I., K.T., H.O., and T.M. analyzed data; and Y.I., S.N., and T.M. wrote the paper.

The authors declare no conflict of interest.

This article is a PNAS Direct Submission.

Freely available online through the PNAS open access option.

Data deposition: The Gb'myo cDNA sequence has been deposited in DNA Data Bank of Japan (accession no. LC128665).

[1]To whom correspondence may be addressed. Email: noji@tokushima-u.ac.jp or mito.taro@tokushima-u.ac.jp.

This article contains supporting information online at www.pnas.org/lookup/suppl/doi:10.1073/pnas.1600612113/-/DCSupplemental.

www.pnas.org/cgi/doi/10.1073/pnas.1600612113

we demonstrate that *G. bimaculatus* Myoglianin (*Gb*'Myo), a homolog of *Drosophila* Myoglianin (18)/vertebrate GDF8/11 (19), suppresses expression of *Gb'jhamt* in the CA of *G. bimaculatus* to down-regulate JH production. Conversely, up-regulation of JH is achieved by *G. bimaculatus* Decapentaplegic (*Gb*'Dpp) and *G. bimaculatus* Glass-bottom boat/60A (*Gb*'Gbb), members of the TGF-β family, as part of a signaling pathway that mediates transcriptional activation of *Gb'jhamt*. Together, these findings provide a paradigm with which we can better understand the endocrine control of invertebrate developmental processes.

Results

In *Drosophila melanogaster* (*Dm*), it was reported that loss of *Dm'mad*, *Dm'tkv*, or *Dm'dpp* caused precocious metamorphosis, even in the early larval stages (20). Therefore, we first examined whether Dpp signaling plays a role in regulating *Gryllus* metamorphosis. For these studies, RNAi targeting *Gb'mad*, *Gb'tkv*, and Common mediator (Co)-Smad (*Gb'medea*) were individually injected into third-instar nymphs. The nymphs that received RNAi targeting *Gb'mad* or *Gb'tkv* achieved adult metamorphosis at the seventh instar rather than the eighth instar in both sexes [male $n = 12/15$, female $n = 14/16$ for *Gb'mad* (Fig. 1*A*) and male $n = 10/12$, female $n = 12/15$ for *Gb'tkv* (Fig. 1*B*)]. In addition, an overall reduction in body size and weight were observed for both RNAi-treated nymphs (Fig. 1 *C* and *D*).

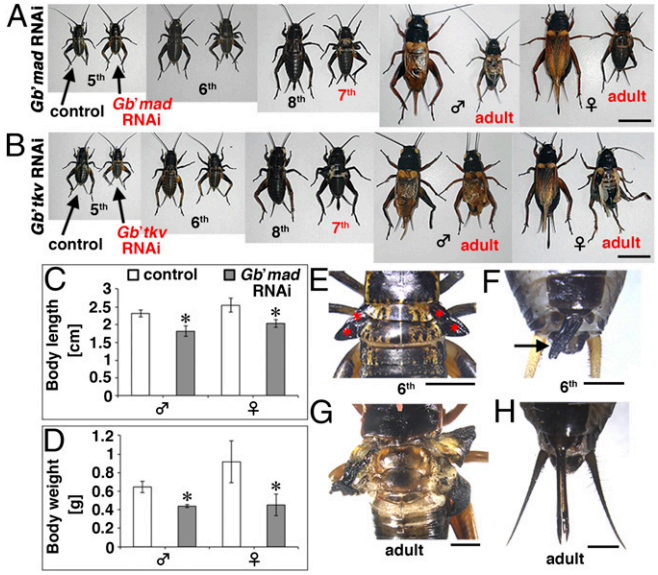

Fig. 1. Phenotypes observed after depletion of *Gb'mad* and *Gb'tkv* was achieved with RNAi in the nymph stage of *G. bimaculatus*. (*A* and *B*) The effects of RNAi targeting *Gb'mad* or *Gb'tkv* in nymphs on day 1 of the third instar. In each box, the control nymph is on the left, and the RNAi-treated nymph is on the right. The instar and adult stages for each box are indicated at the bottom. The RNAi-treated nymphs remained small but underwent precocious adult metamorphosis at the seventh instar. (*C* and *D*) Body length (*C*) and weight (*D*) of male (♂) and female (♀) adults that developed following injections of RNAi targeting *DsRed2* (as a control) or *Gb'mad*. The data presented are the mean ± SD. $*P < 0.05$ according to Student's *t* test. (*E*) The wing pads (indicated by red asterisks) of the sixth-instar *Gb'mad* RNAi nymphs exhibited abnormal growth and displayed an extended side. (*F*) The morphology of the ovipositor (indicated by arrows) in the *Gb'mad* RNAi sixth-instar nymphs was smaller than that of the control nymphs (Fig. 2*O* and Fig. S4*J*). (*G*) Precocious adults were produced following the injection of RNAi targeting *Gb'mad*. The wings of these adults were significantly smaller than those of controls and were wrinkled. (*H*) The ovipositors of the adults produced following the injection of RNAi targeting *Gb'mad* were cleaved at the tip and became abnormally short. (Scale bars: 10 mm in *A* and *B*; 2 mm in *E*, *G*, and *H*; 1 mm in *F*.)

Following the injection of RNAi targeting *Gb'mad,* dysgenesis of the wing pads (Fig. 1 *E* and *G*) and ovipositor (Fig. 1 *F* and *H*) were observed during the sixth instar and the precocious adult stage. Finally, RNAi-mediated depletion of *Gb'medea* led to precocious adult metamorphosis that occurred at the seventh instar ($n = 10/21$). As a result, malformation of the wing pads (Fig. S1 *D* and *E*) and ovipositor (Fig. S1*F*) were observed compared with the control nymphs treated with RNAi targeting *DsRed2* ($n = 31$) (Fig. S1 *A*–*C*).

On the other hand, we identified three different *Gryllus* bone morphogenetic protein (BMP) homologs, *Gb'dpp* (BMP2/4 homolog), *Gb'dpp*-like1 (BMP2-like homolog), and *Gb'dpp*-like2 (BMP3 homolog). Therefore, each of these homologs were targeted with RNAi [*Gb'dpp*, $n = 33$; *Gb'dpp*-like1, $n = 29$; and *Gb'dpp*-like2, $n = 31$]. Combinations of these homologs also were targeted: *Gb'dpp* + *Gb'dpp*-like1 ($n = 25$), *Gb'dpp* + *Gb'dpp*-like2 ($n = 28$), *Gb'dpp*-like1 + *Gb'dpp*-like2 ($n = 27$), and *Gb'dpp* + *Gb'dpp*-like1 + *Gb'dpp*-like2 ($n = 28$). However, all the nymphs that received these RNAi treatments developed normally to become adults (Fig. S1*M*). It is possible that the absence of an effect in these experiments may be caused by the presence of other redundant ligands.

To identify ligands that may be redundant for *Gb'dpp*, RNAi was used to target various *Gryllus* homologs of the *Drosophila* TGF-β family members (21), including *Gb'gbb*, *activinβ* (*Gb'actβ*), *maverick* (*Gb'mav*), and *myoglianin* (*Gb'myo*).

First, we investigated whether depletion of *Gb'gbb* mRNA could be linked to the effects associated with loss of *Gb'tkv, Gb'mad*, or *Gb'medea*. Following the injection of RNAi targeting *Gb'gbb* into third-instar nymphs, precocious differentiation of adult features was observed, and these features were similar to those exhibited by the nymphs that underwent depletion of *Gb'mad* or *Gb'medea* by RNAi. However, substantially fewer *Gb'gbb*-depleted nymphs were obtained ($n = 6/33$) (Fig. S1 *G*–*I*). Because Gbb forms a heterodimeric complex with Dpp in *Drosophila* (22–24), we hypothesized that the simultaneous depletion of *Gb'dpp* and *Gb'gbb* would be sufficient to impair normal adult development, especially in the wing pads and ovipositor. Therefore, we next injected RNAi targeting *Gb'dpp* and RNAi targeting *Gb'gbb* into third-instar nymphs. Of a total of 16 nymphs, 14 exhibited precocious adult metamorphosis. Furthermore, the wing pads and ovipositors of the resulting sixth-instar nymphs and precocious adults resembled those of the nymphs that received RNAi targeting *Gb'mad* or *Gb'medea* (Fig. S1 *J*–*L*). In contrast, the combined targeting of *Gb'dpp*-like1/2 and *Gb'gbb* with RNAi did not affected the ratio of appearance of precocious adult metamorphosis (*Gb'dpp*-like1 + *Gb'gbb*, $n = 2/15$ and *Gb'dpp*-like2 + *Gb'gbb*, $n = 4/17$). Overall, these results demonstrate that the Dpp signaling pathway is triggered by heterodimeric ligand complexes of Dpp and Gbb and that Dpp/Gbb signaling via Tkv and Mad/Medea is critical for ensuring the completion of adult metamorphosis.

When RNAi targeting *myoglianin* was injected into third-instar nymphs, a supernumerary nymphal molt was observed in 52 of 59 of the injected nymphs. In comparison, the control nymphs injected with RNAi targeting *DsRed2* ($n = 33$) underwent normal molting between the fourth and eighth instars and then became adults (Fig. 2*A*; see also Fig. S4*N*). The molting of the *myoglianin*-targeted nymphs specifically involved a progression series of third–3′–3′′–fourth–4′–4′′–fifth instar or third–3′–fourth–4′–4′′–4′′′–fifth instar (instead of third–fourth–fifth instar); they then underwent a sixth-instar molt (Fig. 2 *A* and *B*). We subsequently identified the *myoglianin* homolog as metamorphosis-inducing factor (*Gb'myo*), and its predicted amino acid sequence contains hallmarks of the TGF-β family members (Fig. S2 *A*–*C*). Moreover, although the injection with RNAi targeting *Gb'myo* blocked the morphological transition from one nymphal instar to the next, the number of supernumerary molts at each instar was restricted to

DEVELOPMENTAL BIOLOGY

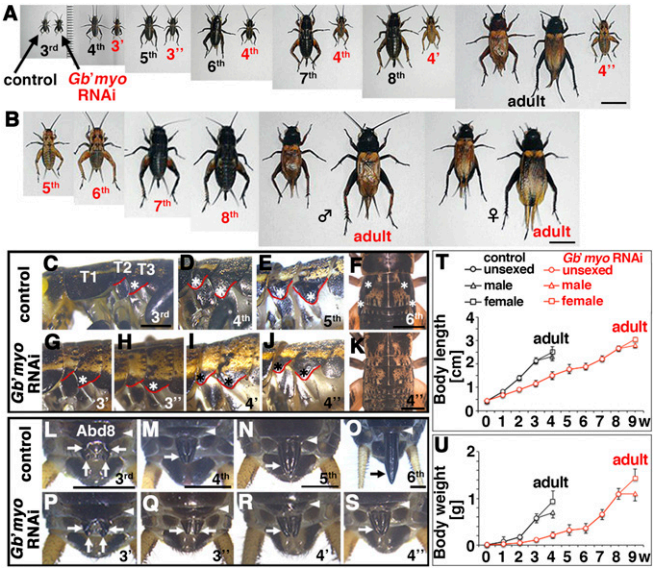

Fig. 2. Phenotypes observed after depletion of *Gb'myo* was achieved with RNAi in *G. bimaculatus*. (*A* and *B*) RNAi targeting *DsRed2* (control) or *Gb'myo* were injected into third-instar nymphs on day 1. Morphological variations during supernumerary molts (3′–3′′–fourth–4′–4′′) and during metamorphosis were subsequently observed in *A* and *B*, respectively. In *A*, the control nymph is on the left and the RNAi-treated nymph is on the right in each box. The instar and adult stages for each box are indicated at the bottom (male: ♂; female: ♀). (*C–E*) Lateral views of third- (*C*), fourth- (*D*), and fifth- (*E*) instar nymphs injected with RNAi targeting *DsRed2* on day 1 of the third instar. The red lines indicate the contours of the wing pads (indicated by asterisks). T1–3; thorax 1–3. (*F*) Dorsal view of the wing pads (indicated by asterisks) in a representative sixth-instar nymph injected with RNAi targeting *DsRed2* on day 1 of the third instar. (*G–J*) Lateral views of supernumerary 3′- (*G*), 3′′- (*H*), 4′- (*I*), and 4′′- (*J*) instar nymphs injected with RNAi targeting *Gb'myo* on day 1 of the third instar. (*K*) Dorsal view of a representative supernumerary 4′′-instar nymph injected with RNAi targeting *Gb'myo* on day 1 of the third instar. (*L–O*) Ventral views of third- (*L*), fourth- (*M*), fifth- (*N*), and sixth- (*O*) instar nymphs injected with RNAi targeting *DsRed2* on day 1 of the third instar. Morphological alterations in the ovipositors (indicated by arrows) at the abdomen 8 (Abd8; indicated by arrowheads) were observed. (*P–S*) Ventral views of supernumerary 3′- (*P*), 3′′- (*Q*), 4′- (*R*), and 4′′- (*S*) instar nymphs injected with RNAi targeting *Gb'myo* on day 1 of the third instar. (*T* and *U*) Body length (*T*) and weight (*U*) of nymphs and adults treated with RNAi targeting *DsRed2* (black) or *Gb'myo* (red). Weeks postinjection (w) are indicated on the *x* axis. The data presented are the mean ± SD. (Scale bars: 10 mm in *A* and *B*; 0.5 mm in *C* and *L–O*; 2 mm in *F* and *K*.)

one to three molts. Moreover, when the sixth-instar nymphs became adults after these supernumerary molts, their body size and weight were significantly greater than those of the controls (Fig. 2 *B*, *T*, and *U*), and the developmental period for metamorphosis was approximately twice that of the controls (see also Fig. S4*N*). However, progressive morphogenesis of the wing pads (Fig. 2 *G–K*) and the ovipositor primordial (Fig. 2 *P–S*) remained unchanged in the supernumerary nymphs over an extended period, whereas the control nymphs developed normal wing pads (Fig. 2 *C–F*) and ovipositors (Fig. 2 *L–O*). Furthermore, when RNAi targeting the TGF-β signaling factor *smox*/*Smad2* (*Gb'smox*) (Fig. S3 *A*, *D*, and *E*; $n = 17/22$) and RNAi targeting the type I receptor *baboon* (*Gb'babo*) (Fig. S3*B*) ($n = 10/15$) were injected into third-instar nymphs, phenotypes similar to those associated with the control nymphs were observed. Based on these RNAi results, targeting of *Gb'myo*, *Gb'babo*, and *Gb'smox* appears to preserve the status quo, and after molting wings and ovipositors are able to form normally, possibly because of the loss of the RNAi effects.

To investigate further the status quo preservation that characterized the RNAi targeting of *Gb'myo*, a second dose of RNAi targeting *Gb'myo* was injected into fourth-instar nymphs (Fig. S4 *A–C*) ($n = 15/15$ for), into fifth-instar nymphs (Fig. S4 *D*, *G*, and *H*) ($n = 14/15$), and into sixth-instar nymphs (Fig. S4 *K* and *L*) ($n = 10/10$) within the first 24 h after ecdysis. Changes in the wing pads and ovipositor for these stages (Fig. S4 *E–L*) and in the relative amounts of *Gb'myo* transcripts (Fig. S4*M*) and the temporal profile of these changes (Fig. S4*N*) suggest that *Gb'myo* may determine the molting characteristics that occur between different nymphal instars. Furthermore, loss of the functions mediated by the *Gb*'Myo protein resulted in developmental arrest and death at the sixth instar.

Methoprene is an analog of JH, and it also was applied to nymphs during the third instar. This treatment resulted in supernumerary molting and larger adults (Fig. S3 *C–E*) ($n = 17/23$). A similar phenotype was observed for the nymphs that received *Gb'myo*-targeted RNAi. Therefore, we hypothesized that *Gb'myo*-RNAi phenotype might be caused by a constant JH titer.

To examine a potential dependence of nymphal instars on the concentration of JH in the hemolymph, JH III production was monitored. Periodic changes in JH III production were observed (Fig. 3*A*), and at the final (eighth) instar, the titer of JH III declined to a low level on day 1 and then was not synthesized until day 7 to allow adult molting (Fig. 3*A*). To examine further whether periodic changes in the JH III titer depended on *Gb*'Myo function, JH III titers were quantified on day 5 for the supernumerary (3′ and fourth) instars that had received RNAi targeting *Gb'myo*. Loss of *Gb'myo* mRNA resulted in constitutively higher JH III titer levels, whereas the introduction of RNAi targeting *Gb'mad* lowered the JH III titer levels only on day 1 of the fourth and sixth instars (Fig. 3*B*). In combination, these data suggest that *Gb*'Mad and *Gb*'Myo play crucial roles in controlling JH biosynthesis.

To investigate the spatial and temporal expression patterns of *Gb'myo* mRNA, quantitative RT-PCR (qPCR) was performed. *Gb'myo* mRNA was found to be highly expressed in the head and thorax 1 (Fig. S5*A*), but the levels of *Gb'myo* mRNA exhibited periodic changes in each of the instars, with a peak in *Gb'myo* mRNA detected on day 3 (Fig. 3*C*). Although stepwise increases in the levels of *Gb'myo* mRNA were observed throughout the developmental stages, they were not observed in adulthood. Moreover, the levels of *Gb'myo* mRNA exhibited no obvious differences between males and females during all nymphal and adult stages. When the levels of *Gb'jhamt* mRNA were detected, peaks in expression were initially observed on day 1 in each instar, decreased by day 3, and then disappeared completely on the day before molting (Fig. 3*E*). This pattern may be associated with the ecdysis process, which is closely tied to the JH cycle. In contrast, *Gb'dpp* mRNA was found to be constitutively expressed in the head throughout the nymphal stages (Fig. 3*D*). A slight change was observed in the transcript levels of *Gb'CYP15A1*, a cytochrome P450 gene that is essential for JH biosynthesis (25); the highest transcript levels were detected in the eighth-instar females (Fig. 3*F*). These results suggest that although *Gb'dpp* may play a role in regulating *Gb'jhamt* expression, *Gb'myo* appears to act as a rate-limiting factor in the *Gb'jhamt* expression pathway.

The spatial expression patterns of *Gb'myo*, *Gb'babo*, *Gb'dpp*, *Gb'tkv*, *Gb'jhamt*, and *Gb'CYP15A1* also were detected in the head with whole-mount in situ hybridization. All these genes were found to be predominantly expressed in the CA on day 3 of the seventh instar (Fig. 3 *G–M*). Similar results were obtained when the transcripts of these genes were detected in the CA by qPCR (Fig. 3 *N* and *O*). Thus, it appears that expression of *Gb'myo* in the CA correlates with the regulation of *Gb'jhamt* expression and JH biosynthesis.

Because both *Gb'myo* and *Gb'dpp* were found to be expressed in the CA, we investigated whether these genes are involved in the regulation of *Gb'jhamt* transcription. First, we confirmed that RNAi targeting of *Gb'myo* was effective in the heads of supernumerary nymphs (Fig. 4*A*). An increase in *Gb'jhamt* expression

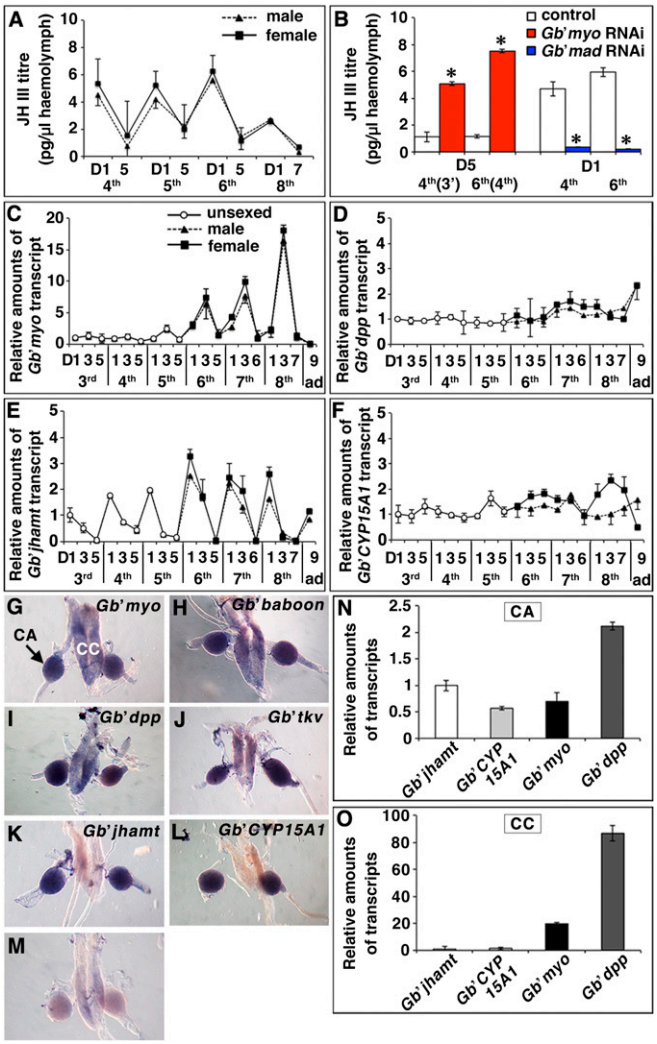

Fig. 3. Expression profiles of *Gb'myo*, *Gb'dpp*, *Gb'jhamt*, and *Gb'CYP15A1* transcripts in *G. bimaculatus* during development and the effect of RNAi targeting *Gb'myo* and *Gb'mad* on the hemolymph titer of JH. (*A*) Developmental changes in JH III titer in the hemolymph of male (dotted line) and female (solid line) nymphs that were collected from the fourth to the eighth instars. (*B*) JH III titer measurements in the hemolymph of nymphs treated with RNAi targeting *Gb'myo* (red) or *Gb'mad* (blue) in the third instar. Asterisks represent significant differences between control and RNAi nymphs: $*P < 0.05$ according to Student's *t* test. (*C*–*F*) Temporal expression of *Gb'myo* (*C*), *Gb'dpp* (*D*), *Gb'jhamt* (*E*), and *Gb'CYP15A1* (*F*) as detected in qPCR analyses of nymph heads. Relative fold changes in the mRNA levels were plotted, and the average expression level in the heads on day 1 of the third instar (D1 third) was set to 1. The mRNA levels were also normalized to *Gb'β-actin* mRNA levels. Developmental stages were defined as days (D) after molting. Nymphs were unsexed during the third to fifth instars and were sexed during the sixth to eighth instars and the adult (ad) stage (male data: dotted lines; female data: solid lines). The data presented are the mean ± SD. (*G*–*M*) Expression levels of *Gb'myo* (*G*), *Gb'baboon* (*H*), *Gb'dpp* (*I*), *Gb'tkv* (*J*), *Gb'jhamt* (*K*), and *Gb'CYP15A1* (*L*) in the corpus allatum–corpus cardiacum (CA–CC) complex on day 3 of the seventh instar were examined by whole-mount in situ hybridization. A control experiment using the *Gb'myo* sense probe is shown in *M*. (*N* and *O*) Expression levels of *Gb'myo*, *Gb'dpp*, *Gb'jhamt*, and *Gb'CYP15A1* as detected in qPCR analyses of RNA samples collected from the CA (*N*) and CC (*O*) of seventh-instar nymphs. The expression level of *Gb'jhamt* was set to 1. The data presented are the mean ± SD.

also was detected in the supernumerary instars on day 1 (3′–fourth–4′), and these levels were significantly higher in these supernumerary nymphs on day 5 as compared with the undetectable levels of *Gb'jhamt* that characterized the controls (Fig. 4*B*). Consistent with the supernumerary molting of the nymphs that had received RNAi targeting *Gb'smox*, *Gb'jhamt* mRNA levels were up-regulated in 3′- and fourth-instar nymphs on day 5 (Fig. S5*B*). In contrast, no significant changes were observed in each of the supernumerary instars that expressed the *Gb'CYP15A1* transcript (Fig. 4*C*). When RNAi targeting *Gb'mad* (Fig. 4*D*), *Gb'medea* (Fig. S5*C*), or *Gb'gbb* (Fig. S5*D*) was injected into third-instar nymphs, *Gb'jhamt* transcript levels were lower in both the fourth- and sixth-instar nymphs on day 1, whereas no apparent effect on *Gb'CYP15A1* mRNA levels were observed in the *Gb'mad*-depleted nymphs (Fig. 4*D*). Taken together, these results demonstrate that the precocious metamorphosis in nymphs that received RNAi targeting *Gb'mad*, *Gb'medea*, or *Gb'gbb* derives from repression of *Gb'jhamt* expression, and they also suggest that the up-regulation of *Gb'jhamt* in nymphs that received RNAi targeting *Gb'myo* or *Gb'smox* may depend on timely regulation of the *Gb*'Dpp/Gbb signaling pathway.

Following the injection of RNAi targeting *Gb'jhamt* into third-instar nymphs, precocious metamorphosis was observed, and these features were similar to those of RNAi depletion targeting *Gb'mad* (Fig. S6*A*). To examine whether the increase in *Gb'jhamt* expression caused by *Gb'myo*-targeted RNAi can be prevented by the knockdown of *Gb'mad* or *Gb'jhamt*, *Gb'myo* RNAi + *Gb'mad* RNAi and *Gb'myo* RNAi + *Gb'jhamt* RNAi were injected into third-instar nymphs ($n = 9/12$ and $n = 15/16$, respectively; Fig. S6 *B* and *C*). Changes in overall body size (Fig. S6 *D* and *E*) and relative transcript levels (Fig. S6*F*) were observed. Moreover, the supernumerary molting phenotype was rescued when *Gb'jhamt* was targeted for depletion. Thus, it appears that supernumerary molts are caused by alterations in *Gb'jhamt* expression. However, the mechanisms underlying regulation of *Gb'jhamt* expression by *Gb*'Myo signaling are unknown.

In recent studies, the transcriptional repressor Brinker (Brk) has been found to be a Dpp target that negatively regulates Dpp signaling in *Drosophila* (26, 27). Therefore, we examined the levels of *Gb'brk* mRNA in nymphs that received RNAi targeting genes related to *Gb*'Dpp/Gbb signaling (*Gb'mad*, *Gb'medea*, and *Gb'gbb*) or *Gb*'Myo signaling (*Gb'myo* and *Gb'smox*). In the former experiments, depletion of *Gb'mad* (Fig. 4*E*), *Gb'medea* (Fig. S5*C*), and *Gb'gbb* (Fig. S5*D*) resulted in an increase in *Gb'brk* mRNA levels in fourth- and sixth-instar nymphs on day 1. These results suggest that *Gb'brk* expression is negatively regulated by Gb'Dpp/Gbb signaling (Fig. 5*A*). Thus, we speculated that the transcriptional repressor Gb'Brk plays a role in negatively regulating Gb'Dpp/Gbb signaling, and it may regulate the repression of *Gb'jhamt*. To examine the latter possibility, RNAi targeting *Gb'brk* was injected into third-instar nymphs. Although the control animals exhibited normal molting, the majority (25 of 27) of the *Gb'brk* RNAi-treated nymphs arrested in the early developmental stages. In addition, increased expression of *Gb'jhamt* mRNA was detected in the *Gb'brk* RNAi-treated nymphs during the fourth and sixth instars on day 1, but no effect was observed on day 5 (Fig. 4*F*). These results suggest that *Gb*'Brk may be associated with the negative regulation of *Gb'jhamt* (Fig. 5*B*). To investigate whether the reduction in *Gb'jhamt* expression in the *Gb'mad*-depleted nymphs was caused by concomitant up-regulation of *Gb'brk* (Fig. 5*A*), dual RNAi targeting *Gb'mad* and *Gb'brk* were injected into third-instar nymphs. Subsequently, *Gb'mad* RNAi-dependent repression of *Gb'jhamt* that previously was observed in the fourth and sixth instars on day 1 was not rescued by depletion of *Gb'brk* (Fig. 4*F*). Thus, repression of *Gb'jhamt* in the nymphs that received RNAi targeting *Gb'mad* appeared to be independent of increased *Gb'brk* expression (Fig. 5*C*). Consequently, our results suggest that both an up-regulation of *Gb'jhamt* and a down-regulation of *Gb'brk* are controlled by the *Gb*'Dpp/Gbb/Mad signaling pathway (Fig. 5 *D* and *F*). *Gb'brk* expression was markedly decreased on days 1 or 5 in the supernumerary nymphs (3′ and fourth instars) with depletion of *Gb'myo* (Fig. 4*E*) and *Gb'smox* (Fig. 5*D* and Fig. S5*B*). Therefore,

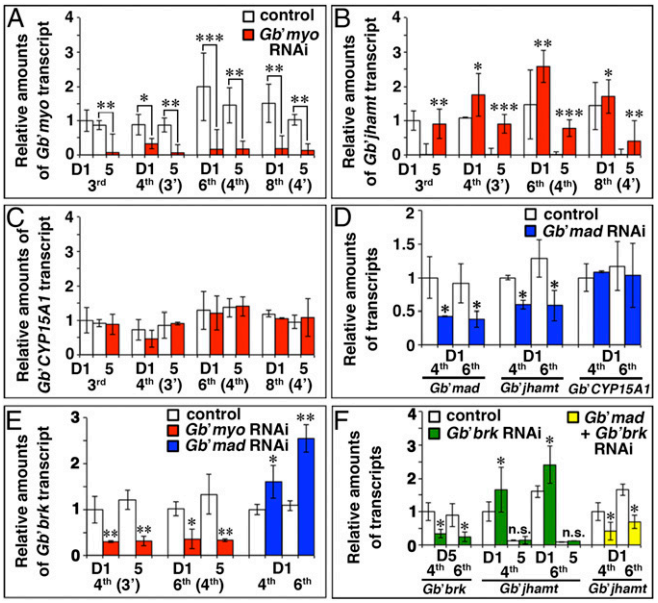

Fig. 4. The effects of RNAi-mediated depletion of *Gb'myo* and *Gb'mad* on the expression of *Gb'jhamt*, *Gb'CYP15A1*, and *Gb'brk*. (*A–C*) RNAi targeting *DsRed2* control or *Gb'myo* were injected on day 1 of the third instar. Transcript levels of *Gb'myo* (*A*), *Gb'jhamt* (*B*), and *Gb'CYP15A1* (*C*) were subsequently determined on days 1 and 5 in the heads of the supernumerary third-, 3′-, fourth-, and 4′-instar nymphs. The transcript levels determined on day 1 of the third-instar control nymphs (D1 third) for *A–C* were set to 1. The data presented are the mean ± SD. (*D*) Transcript levels of *Gb'mad*, *Gb'jhamt*, and *Gb'CYP15A1* also were determined on day 1 of the fourth and sixth instars following the injection of RNAi targeting *Gb'mad*. The transcript levels of these genes in control nymphs on day 1 of the fourth instar (D1 fourth) were set to 1. The data presented are the mean ± SD. (*E*) *Gb'brk* mRNA levels in the heads of fourth- (3′) and sixth- (fourth-) instar nymphs on days 1 and 5 after the injection of RNAi targeting *Gb'myo* (red) and on day 1 for the fourth- and sixth-instar nymphs that received RNAi targeting *Gb'mad* (blue). The transcript levels of both sets of control nymphs on day 1 of the fourth instar were set to 1. The data presented are the mean ± SD. (*F*) After RNAi-mediated depletion of *Gb'brk* (green) or *Gb'mad* + *Gb'brk* (yellow) in the third instar, transcript levels of *Gb'brk* or *Gb'jhamt* were measured on days 1 and 5 of the fourth and sixth instars as indicated. The transcript levels measured on day 5 (D5 fourth) or day 1 (D1 fourth) of the control fourth-instar nymphs, respectively, were set to 1. The data presented are the mean ± SD. Asterisks in *A*, *B*, and *D–F* represent significant differences between the control and RNAi nymphs. n.s., not significant; **P* < 0.05; ***P* < 0.005; ****P* < 0.001 according to Student's *t* test.

we propose that induction of *Gb'jhamt* and repression of *Gb'brk* that are dependent on the function of *Gb*'Mad may be blocked by *Gb*'Myo/Smox signaling (Fig. 5 *E* and *F*).

Previous studies have showed that *Daughters against dpp* (*dad*) is an inhibitory Smad that is able to antagonize Dpp signaling genetically in *Drosophila* (28). Regulation of *dad* also has been reported to be affected by the function of Mad and Smox (29). To understand how *Gb*'Myo signaling prevents *Gb*'Dpp/Gbb signaling, we investigated whether the *Gb*'Dpp/Gbb and *Gb*'Myo signaling pathways are associated with expression of *Gb'dad*. When RNAi targeting *Gb'mad* was injected into third-instar nymphs, lower levels of *Gb'dad* mRNA were detected (Fig. S5*E*). In contrast, depletion of *Gb'smox* by RNAi had no effect on *Gb'dad* expression (Fig. S5*E*). These results suggest that *Gb'dad* may represent a target gene downstream of *Gb*'Dpp/Gbb signaling and that *Gb*'Myo signaling may regulate the expression of *Gb'brk* and *Gb'jhamt* through the control of the *Gb*'Dpp/Gbb signaling pathway (Fig. 5 *E* and *F*).

Overall, the results of the experiments performed suggest that *Gb*'Myo signaling suppresses *Gb'jhamt* expression that is induced by *Gb*'Dpp/Gbb signaling and that this suppression leads to an inhibition of JH biosynthesis and an induction of metamorphosis.

Discussion

The results of the present study demonstrate that the TGF-β ligands *Gb*'Dpp, *Gb*'Gbb, and *Gb*'Myo regulate the synthesis of JH by regulating the expression of *Gb'jhamt* in the CA (Fig. 5*F*). As part of this process, transcription of the *jhamt* gene is controlled by the Dpp/Gbb/Tkv/Mad/Medea signaling pathway, and Myo/Babo/Smox signaling suppresses *jhamt* expression by controlling the Dpp/Gbb/Tkv/Mad/Medea signaling pathway. Expression of JHAMT in CA cells transforms JH acid into JH, and the latter is released into the hemolymph (Fig. 5*F*). We hypothesize that these regulatory mechanisms that determine the titer of JH are common in insects, including holometabola, for four reasons: because (*i*) the CA is a common endocrine gland which generates JH in insects; (*ii*) *Gb*'Dpp functions in the CA similarly to *Dm*'Dpp in the CA of *Drosophila* (20); (*iii*) *Dm*'Myo, a homolog of *Gb*'Myo, is secreted by glial cells before metamorphosis to direct developmental neural remodeling (30); and (*iv*) *Gb'myo* regulates final insect size by regulating the JH titer as observed in *Drosophila* (31).

However, RNAi treatment is not equivalent to genetic knockdown; therefore, because of incomplete knockdown, it may not be possible to demonstrate the precise regulatory relationship between *smox*, *mad*, *brk*, and *jhamt*. In addition, RNAi knockdown occurs throughout the whole body and cannot be specifically targeted to the CA. Thus, the knockdown of these genes by RNAi may occur in other tissues. For example, *Gb'myo* and *Gb'dpp* also are expressed in the brains of *G. bimaculatus* nymphs (Fig. S5*F*), and the mechanisms that regulate Dpp and Myo production in the brain remain to be determined. It has been proposed that allatotropic and allatostatic peptides may play a role (9, 32). However, the phenotypes observed following targeting of the allatostatin-A type gene by RNAi (33) differ from the phenotypes generated by *Gb'myo* RNAi but are similar to the phenotypes obtained following the up-regulation of JH. Thus, no significant relations between allatostatins and Myo have been identified. On the other hand, in the *Drosophila* prothoracic gland, knockdown of the *Activin/Babo/Smox* pathway causes developmental arrest before metamorphosis through the control the ecdysone biosynthesis through the regulation of PTTH and insulin-signaling pathways (34). Our results show that

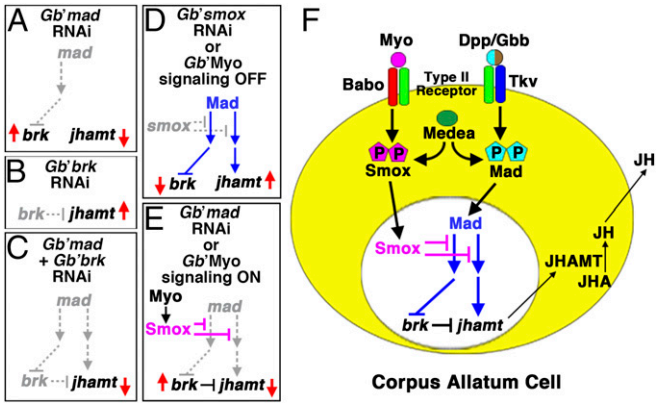

Fig. 5. Regulation of *Gb'jhamt* expression. (*A–E*) Schematic diagrams of *Gb'brk* and *Gb'jhamt* transcriptional regulation based on the results obtained from experiments targeting *Gb'mad* (*A* and *E*), *Gb'brk* (*B*), *Gb'mad* + *Gb'brk* (*C*), and *Gb'smox* (*D*) genes by RNAi. Gray denotes gene depletion and transcriptional regulatory effects by RNAi. Red arrows indicate the down- and up-regulation of target gene expression. (*F*) A diagram depicting the function of Dpp/Gbb (blue) and Myo (pink) signaling pathways in the regulation of *jhamt* expression and JH action. P indicates the phosphorylation of Mad and Smox.

in *G. bimaculatus* nymphs, *Gb'myo* is also expressed in the thorax 1 (prothorax) including the prothoracic gland (Fig. S5*A*). Thus, *Gb*'Myo/Babo/Smox signaling may be independently associated with both JH and ecdysone biosynthesis. It should be noted, however, that as yet no connection between *Gb*'Myo and ecdysone biosynthesis has been established in this study. Finally, in mice, Myostatin/GDF8, a homolog of *Gb*'Myo, is a potent inhibitor of skeletal muscle growth (19), and another homolog of GDF11 has been reported to inhibit muscle formation (35, 36). Thus, GDF8/11 function might be an important regulator of adult muscle size. These GDF members are likely to be evolutionarily conserved as a body-size regulator among animals.

In conclusion, the present findings provide common regulatory mechanisms with TGF-β signaling to explain the endocrine control of invertebrate life cycles. We anticipate that further studies on regulation of the *Gb*'Myo signaling in the brain and prothoracic gland will be of great interest.

Materials and Methods

Animals. All adult and nymph two-spotted *G. bimaculatus* crickets were reared at 29 °C and 50% humidity under standard conditions, as previously described (37).

Cloning. *Gryllus* genes related to Dpp/Myo-signaling genes were cloned by RT-PCR from third-instar nymph cDNA samples using the gene-specific primers listed in Table S1. A putative full-length cDNA sequence containing the ORF of *Gb'myo* (864 bp) was deposited in the DNA Data Bank of Japan (accession no. LC128665). RT-PCR was done as described in *SI Materials and Methods*.

RNAi. The synthesis of RNAi was performed as described in *SI Materials and Methods*. Within 24 h after ecdysis, nymphs were injected with 20 μM RNAi in a volume of 0.2–0.5 μL into the ventral abdomen. RNAi targeting *DsRed2* was injected as a negative control. In the dual RNAi experiments, a combination of RNAi targeting *Gb'myo* and *Gb'jhamt*, *Gb'myo* and *Gb'mad*, *Gb'mad* and *Gb'brk*, or *Gb'dpp* and *Gb'gbb*, each with a final concentration of 20 μM, were injected.

qPCR. The qPCR primers used are listed in Table S2. RNA extraction, cDNA synthesis, and qPCR conditions are described in *SI Materials and Methods*.

In Situ Hybridization. Digoxigenin-labeled antisense RNA probes for *Gb'myo*, *Gb'babo*, *Gb'dpp*, *Gb'tkv*, *Gb'jhamt*, and *Gb'CYP15A1* cDNA fragments obtained by RT-PCR were used for whole-mount in situ hybridization. In situ hybridization was performed as described in *SI Materials and Methods*.

JH Extraction. *G. bimaculatus* nymphs were dissected,and hemolymph (~5 μL per nymph) was extracted using methanol/isooctane (1:1, vol/vol) with 50 ng fenoxycarb (Wako Pure Chemical Industries) as an internal standard. Additional procedures for JH extraction are described in *SI Materials and Methods*.

LC-MS. An ultra performance liquid chromatography (UPLC)-LCT Premier system (Waters) was equipped with a 50×2.1 mm^2 C_{18} reverse-phase column (ACQUITY UPLC BEH ODS-1.7 μm; Waters) that was protected by a VanGuard Pre-Column (Waters) and eluted with 100% (vol/vol) methanol at a flow rate of 0.3 mL/min. MS analysis was performed as described in *SI Materials and Methods*.

Hormone Treatment. A JH analog, methoprene, was dissolved in ethanol (Wako Pure Chemical Industries) to a concentration of 100 μg/μL. Then, ~0.2 μL of this methoprene solution was injected into the ventral abdomen of newly molted third- or fifth-instar nymphs (~20 μg of methoprene per nymph). The same volume of ethanol was injected as a control.

ACKNOWLEDGMENTS. We thank Prof. Eiji Sakuradani (Tokushima University) for continuous support, and Kayoko Tada, Shoko Ueta, and Etsuko Fujinaga for technical assistance. This work was supported by funding from MEXT/JSPS KAKENHI Grants 22124003/22370080 (to S.N., T.B., H.O., and T.M.) and 25650080/26292176 (to T.M.).

1. Truman JW, Riddiford LM (2002) Endocrine insights into the evolution of metamorphosis in insects. *Annu Rev Entomol* 47:467–500.
2. Belles X (2011) Origin and evolution of insect metamorphosis. *Encyclopedia of Life Sciences* (John Wiley and Sons, Chichester), pp 111–999.
3. Riddiford LM (2012) How does juvenile hormone control insect metamorphosis and reproduction? *Gen Comp Endocrinol* 179(3):477–484.
4. Nijhout HF (1994) *Insect Hormones* (Princeton Univ Press, Princeton).
5. Riddiford LM (1994) Cellular and molecular actions of juvenile hormone. I. General considerations and premetamorphic actions. *Adv Insect Physiol* 24:213–274.
6. Wigglesworth VB (1936) The function of the corpus allatum in the growth and reproduction of *Rhodnius prolixus* (Hemiptera). *Q J Microsc Sci* 79:91–121.
7. Fukuda S (1944) The hormonal mechanism of larval molting and metamorphosis in the silkworm. *J Fac Sci Imp Univ Tokyo. Sec IV* 6:477–532.
8. Goodman WG, Cusson M (2012) The juvenile hormones. *Insect Endocrinology*, ed Gilbert LI (Academic, New York), pp 311–347.
9. Stay B, Tobe SS (2007) The role of allatostatins in juvenile hormone synthesis in insects and crustaceans. *Annu Rev Entomol* 52:277–299.
10. Jindra M, Palli SR, Riddiford LM (2013) The juvenile hormone signaling pathway in insect development. *Annu Rev Entomol* 58:181–204.
11. Niwa R, et al. (2008) Juvenile hormone acid O-methyltransferase in *Drosophila melanogaster*. *Insect Biochem Mol Biol* 38(7):714–720.
12. Minakuchi C, Namiki T, Yoshiyama M, Shinoda T (2008) RNAi-mediated knockdown of juvenile hormone acid O-methyltransferase gene causes precocious metamorphosis in the red flour beetle *Tribolium castaneum*. *FEBS J* 275(11):2919–2931.
13. Li W, et al. (2013) Molecular cloning and characterization of juvenile hormone acid methyltransferase in the honey bee, *Apis mellifera*, and its differential expression during caste differentiation. *PLoS One* 8(7):e68544.
14. Shinoda T, Itoyama K (2003) Juvenile hormone acid methyltransferase: A key regulatory enzyme for insect metamorphosis. *Proc Natl Acad Sci USA* 100(21):11986–11991.
15. Nakamura T, et al. (2010) Imaging of transgenic cricket embryos reveals cell movements consistent with a syncytial patterning mechanism. *Curr Biol* 20(18):1641–1647.
16. Mito T, Noji S (2009) The two-spotted cricket *Gryllus bimaculatus*: An emerging model for developmental and regeneration studies. *CSH Protoc* 1:331–346.
17. Erezyilmaz DF, Riddiford LM, Truman JW (2004) Juvenile hormone acts at embryonic molts and induces the nymphal cuticle in the direct-developing cricket. *Dev Genes Evol* 214(7):313–323.
18. Lo PC, Frasch M (1999) Sequence and expression of myoglianin, a novel *Drosophila* gene of the TGF-β superfamily. *Mech Dev* 86(1-2):171–175.
19. Lee SJ, McPherron AC (1999) Myostatin and the control of skeletal muscle mass. *Curr Opin Genet Dev* 9(5):604–607.
20. Huang J, et al. (2011) DPP-mediated TGFbeta signaling regulates juvenile hormone biosynthesis by activating the expression of juvenile hormone acid methyltransferase. *Development* 138(11):2283–2291.
21. Hevia CF, de Celis JF (2013) Activation and function of TGFβ signalling during *Drosophila* wing development and its interactions with the BMP pathway. *Dev Biol* 377(1):138–153.
22. Bangi E, Wharton K (2006) Dual function of the *Drosophila* Alk1/Alk2 ortholog Saxophone shapes the Bmp activity gradient in the wing imaginal disc. *Development* 133(17):3295–3303.
23. Ballard SL, Jarolimova J, Wharton KA (2010) Gbb/BMP signaling is required to maintain energy homeostasis in *Drosophila*. *Dev Biol* 337(2):375–385.
24. Raftery LA, Umulis DM (2012) Regulation of BMP activity and range in *Drosophila* wing development. *Curr Opin Cell Biol* 24(2):158–165.
25. Daimon T, et al. (2012) Precocious metamorphosis in the juvenile hormone-deficient mutant of the silkworm, *Bombyx mori*. *PLoS Genet* 8(3):e1002486.
26. Campbell G, Tomlinson A (1999) Transducing the Dpp morphogen gradient in the wing of *Drosophila*: Regulation of Dpp targets by brinker. *Cell* 96(4):553–562.
27. Jaźwińska A, Kirov N, Wieschaus E, Roth S, Rushlow C (1999) The *Drosophila* gene *brinker* reveals a novel mechanism of Dpp target gene regulation. *Cell* 96(4):563–573.
28. Tsuneizumi K, et al. (1997) Daughters against dpp modulates dpp organizing activity in *Drosophila* wing development. *Nature* 389(6651):627–631.
29. Peterson AJ, O'Connor MB (2013) Activin receptor inhibition by Smad2 regulates *Drosophila* wing disc patterning through BMP-response elements. *Development* 140(3):649–659.
30. Awasaki T, Huang Y, O'Connor MB, Lee T (2011) Glia instruct developmental neuronal remodeling through TGF-β signaling. *Nat Neurosci* 14(7):821–823.
31. Mirth CK, et al. (2014) Juvenile hormone regulates body size and perturbs insulin signaling in *Drosophila*. *Proc Natl Acad Sci USA* 111(19):7018–7023.
32. Weaver RJ, Audsley N (2009) Neuropeptide regulators of juvenile hormone synthesis: Structures, functions, distribution, and unanswered questions. *Ann N Y Acad Sci* 1163:316–329.
33. Meyering-Vos M, Merz S, Sertkol M, Hoffmann KH (2006) Functional analysis of the allatostatin-A type gene in the cricket *Gryllus bimaculatus* and the armyworm *Spodoptera frugiperda*. *Insect Biochem Mol Biol* 36(6):492–504.
34. Gibbens YY, Warren JT, Gilbert LI, O'Connor MB (2011) Neuroendocrine regulation of *Drosophila* metamorphosis requires TGFbeta/Activin signaling. *Development* 138(13):2693–2703.
35. Kaiser J (2015) Regenerative medicine. 'Rejuvenating' protein doubted. *Science* 348(6237):849.
36. Brun CE, Rudnicki MA (2015) GDF11 and the mythical Fountain of Youth. *Cell Metab* 22(1):54–56.
37. Niwa N, Saitoh M, Ohuchi H, Yoshioka H, Noji S (1997) Correlation between distal-less expression patterns and structures of appendages in development of the two-spotted cricket, *Gryllus bimaculatus*. *Zoolog Sci* 14(1):115–125.